Forest Chemicals Review
www.forestchemicalsreview.com
ISSN: 1520-0191
May-June 2022 Page No. 932-946
Article History: Received: 24 February 2022, Revised: 05 April 2022, Accepted: 08 May 2022, Publication: 30 June 2022

Dynamic Antiplane Behaviour of Radial Collinear Cracks Emanating from Multiple Noncircular Cavities in Piezoelectric Material

Dong Li[1], Huicong Wang[2*], Hongze Tian[3], Yaping Liu[4]
[1]Center for Quality Management, Hebei Jiaotong Vocational and Technical College, Shijiazhuang, Hebei, China
[2]Department of Road and Bridge Engineering, Hebei Jiaotong Vocational and Technical College, Shijiazhuang, Hebei, China
[3]Hebei Jiaotou Intelligent Transportation Technology Co., Ltd, Shijiazhuang, Hebei, China
[4]Department of Rail Transit, Hebei Jiaotong Vocational and Technical College, Shijiazhuang, Hebei, China
*Corresponding Author.

Abstract:

To further clarify the fracture mechanics characteristics of piezoelectric materials with defects, this paper studies the dynamic antiplane problems of radial collinear cracks emanating from multiple noncircular cavities in piezoelectric material. First, the expressions of Green function satisfying the boundary conditions in the semi-infinite piezoelectric medium with multiple depressions of arbitrary shape, the total displacement and the electric potential in the piezoelectric medium containing noncircular cavities and without cracks are derived by using complex variable function method and conformal mapping technology. Then, based on the crack-division technique and conjunction method, the problem is transformed into a set of Fredholm definite integral equations of the first kind. And the direct numerical integration method is used to solve it. As an example, the influences of defect size, SH wave frequency and material parameters on the dynamic stress concentration at the crack tip are given, which provides some theoretical guidance for the engineering design, production and safe use of piezoelectric devices.

Keywords*: Radial cracks, Noncircular cavity, Piezoelectric, Green function, Dynamic analysis.*

I. INTRODUCTION

Piezoelectric materials have good electromechanical coupling, and are widely used as sensors, actuators and other devices. However, the stress and electric field concentration caused by defects such as inclusions, cavities and cracks in use often lead to the loss of its design function. Therefore, many researchers focus on the physical and mechanical mechanism of piezoelectric material fracture in recent years. And many useful results have been achieved which greatly improve the application of piezoelectric materials.

In the aspect of inclusion defects, Du [1], Feng [2], and Hu [3] have made significant efforts to this

Forest Chemicals Review
www.forestchemicalsreview.com
ISSN: 1520-0191
May-June 2022 Page No. 932-946
Article History: Received: 24 February 2022, Revised: 05 April 2022, Accepted: 08 May 2022, Publication: 30 June 2022

topic. In terms of crack defects, Wang[4], Wu [5], Zheng [6], Hu [7] studied the mechanical behavior of cracks under load. In the aspect of crack defects emanating from cavities, García-Sánchez [8], Guo [9], Xiao [10] and Feng [11] studied the stress concentration at the tip of cracks by using mixed boundary element method, complex function, conformal mapping method, etc.

It can be seen that most of the researches on the composite defects of cavities and cracks are static fracture problems, while the research on dynamic fracture mechanics is rarely reported. The theoretical analysis of the dynamic antiplane behavior of radial collinear cracks emanating from multiple cavities is carried out in this paper. The conclusions can provide very useful suggestions for the design, manufacture and engineering application of piezoelectric components.

II. MODEL OF THE PROBLEM

The mechanical model of transversely isotropic piezoelectric material containing radial finite-length cracks emanating from multiple noncircular cavities is shown in Fig 1. The medium contains radial collinear cracks emanating from M noncircular cavities. The coordinate of each cavity center is c_j. The local coordinate system ($x_jo_jy_j$) and (r_jq_j) is established with each cavity center as the origin, and the crack lengths are A_{2j-1} and A_{2j} respectively, where j=1, 2, ..., M. The distances between adjacent cracks are $d_1, d_2, \ldots d_{M-1}$, and the SH wave is incident at a_0 angle with the X axis.

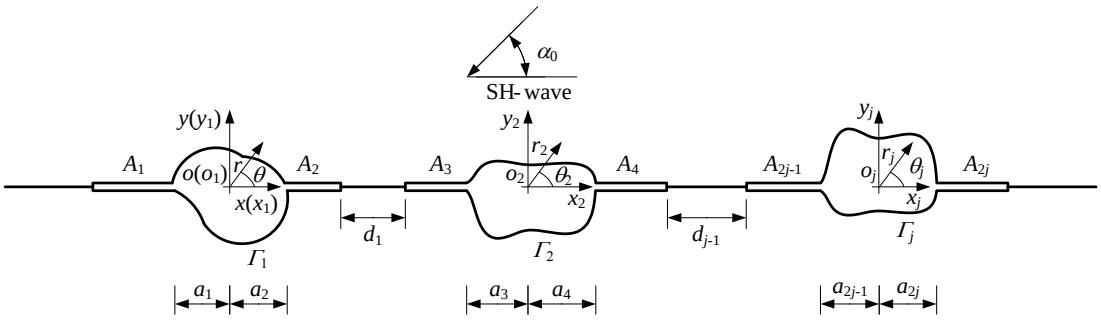

Fig 1: Model of radial collinear cracks emanating from multiple noncircular cavities in piezoelectric material

The boundary conditions of cracks are:

$$\begin{cases} D_\theta^+(\vec{r}) = D_\theta^-(\vec{r}) \\ \tau_{\theta z}^+(\vec{r}) = \tau_{\theta z}^-(\vec{r}) = 0 \\ \phi^+(\vec{r}) = \phi^-(\vec{r}) \end{cases}, \begin{cases} r_j \in [a_{2j-1}, a_{2j-1} + A_{2j-1}], \theta_j = \pi \\ r_j \in [a_{2j}, a_{2j} + A_{2j}], \theta_j = 0 \end{cases} \tag{1}$$

The boundary conditions at the noncircular cavities are:

Forest Chemicals Review
www.forestchemicalsreview.com
ISSN: 1520-0191
May-June 2022 Page No. 932-946
Article History: Received: 24 February 2022, Revised: 05 April 2022, Accepted: 08 May 2022, Publication: 30 June 2022

$$\begin{cases} \tau_{rz}(\vec{r}) = 0 \\ \phi(\vec{r}) = \phi_j^c \quad , \quad |\vec{r}| = \Gamma_j \\ D_r(\vec{r}) = D_{r_j}^c \end{cases} \tag{2}$$

Wherein, f is electric potential field, t_{rz} and t_{qz} are shear stress components, D_r and D_q are electric displacement components; the superscript "+" , "-" and "c" represent the upper and lower surface of the crack, the field quantity of the medium inside the noncircular cavity respectively.

The governing equations of the steady-state antiplane piezoelectric dynamic problem is:

$$\begin{aligned} c_{44}\nabla^2 w + e_{15}\nabla^2\phi + \rho\omega^2 w = 0 \\ e_{15}\nabla^2 w - \kappa_{11}\nabla^2\phi = 0 \end{aligned} \tag{3}$$

Wherein, c_{44}, e_{15} and k_{11} are the elastic constant, the piezoelectric coefficient and the dielectric constant in piezoelectric material; w, r and w represent the displacement field, matter density and circular frequency of SH wave respectively.

Introducing a new function $j(x,y)$[12], which satisfies the following equation, namely:

$$\varphi = \phi - \frac{e_{15}}{\kappa_{11}} w \tag{4}$$

By substituting equation (4) into equation (3), the control equations are decoupled as:

$$\nabla^2 w + k^2 w = 0, \quad \nabla^2\varphi = 0 \tag{5}$$

Wherein, ∇^2 is the Laplace operator, $\nabla^2 = \frac{\partial^2}{\partial x^2} + \frac{\partial^2}{\partial y^2}$; $k^2 = \frac{\rho\omega^2}{c^*}$, and $c^* = c_{44} + \frac{e_{15}^{\ 2}}{\kappa_{11}} = c_{44}(1+\lambda)$.

On complex planes $\eta = re^{i\theta}$ and $\bar{\eta} = re^{-i\theta}$, equation (5) can be given by:

$$\frac{\partial^2 w}{\partial\eta\partial\bar{\eta}} + \frac{1}{4}k^2 w = 0, \quad \frac{\partial^2\varphi}{\partial\eta\partial\bar{\eta}} = 0 \tag{6}$$

Forest Chemicals Review
www.forestchemicalsreview.com
ISSN: 1520-0191
May-June 2022 Page No. 932-946
Article History: Received: 24 February 2022, Revised: 05 April 2022, Accepted: 08 May 2022, Publication: 30 June 2022

$$\begin{aligned}
\tau_{rz} &= c_{44}\left(\frac{\partial w}{\partial \eta}e^{i\theta}+\frac{\partial w}{\partial \bar{\eta}}e^{-i\theta}\right)+e_{15}\left(\frac{\partial \phi}{\partial \eta}e^{i\theta}+\frac{\partial \phi}{\partial \bar{\eta}}e^{-i\theta}\right)\\
\tau_{\theta z} &= ic_{44}\left(\frac{\partial w}{\partial \eta}e^{i\theta}-\frac{\partial w}{\partial \bar{\eta}}e^{-i\theta}\right)+ie_{15}\left(\frac{\partial \phi}{\partial \eta}e^{i\theta}-\frac{\partial \phi}{\partial \bar{\eta}}e^{-i\theta}\right)\\
D_r &= e_{15}\left(\frac{\partial w}{\partial \eta}e^{i\theta}+\frac{\partial w}{\partial \bar{\eta}}e^{-i\theta}\right)-\kappa_{11}\left(\frac{\partial \phi}{\partial \eta}e^{i\theta}+\frac{\partial \phi}{\partial \bar{\eta}}e^{-i\theta}\right)\\
D_\theta &= ie_{15}\left(\frac{\partial w}{\partial \eta}e^{i\theta}-\frac{\partial w}{\partial \bar{\eta}}e^{-i\theta}\right)-i\kappa_{11}\left(\frac{\partial \phi}{\partial \eta}e^{i\theta}-\frac{\partial \phi}{\partial \bar{\eta}}e^{-i\theta}\right)
\end{aligned} \tag{7}$$

III. THEORETICAL SOLUTIONS

3.1 Green function of the problem

The Green function of displacement G_w and electric potential G_f adopts the fundamental solutions when the semi-infinite material with multiple depressions of arbitrary shape is subjected to the out-of-plane line load $\delta(\eta-\eta_0)$ which is in harmony with time at any point η_0 on its horizontal surface. Its model is shown in Fig 2.

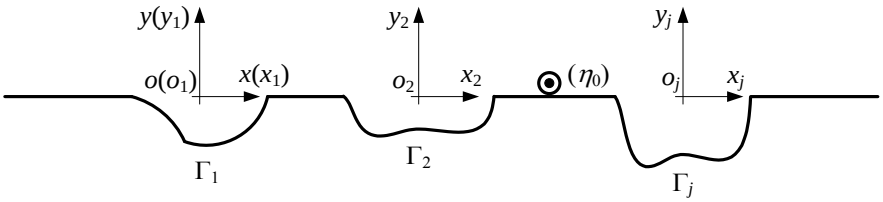

Fig 2: Semi-infinite piezoelectric medium model with multiple depressions of arbitrary shape

The boundary conditions at the depressions of arbitrary shape are:

$$\begin{cases}
\tau_{rz}{}^{j}=0\\
D_r{}^{j}=D_r^{cj}, \quad |\eta_j|=\Gamma_j \quad (j=1,2,\cdots,\mathrm{M})\\
G_\phi{}^{j}=G_\phi^{cj}
\end{cases} \tag{8}$$

On the complex plane $(\eta,\bar{\eta})$, the displacement Green function G_w and the electric potential Green function G_f satisfying the governing equation (6) are composed of incident and scattering parts, which are represented by superscript *i* and *s* respectively. The expressions of the first part are:

$$G_w^{(i)}=\frac{i}{2c_{44}(1+\lambda)}H_0^{(1)}(k|\eta-\eta_0|), \quad G_\phi^{(i)}=\frac{e_{15}}{\kappa_{11}}G_w^{(i)} \tag{9}$$

Forest Chemicals Review
www.forestchemicalsreview.com
ISSN: 1520-0191
May-June 2022 Page No. 932-946
Article History: Received: 24 February 2022, Revised: 05 April 2022, Accepted: 08 May 2022, Publication: 30 June 2022

The scattered wave part can be taken as follows:

$$G_w^{(s)} = \sum_{j=1}^{M} \sum_{n=-\infty}^{\infty} A_n^j H_n^{(1)}(k|\eta_j|) \cdot \left[\left(\frac{\eta_j}{|\eta_j|} \right)^n + \left(\frac{\eta_j}{|\eta_j|} \right)^{-n} \right]$$
$$G_\phi^{(s)} = \frac{e_{15}}{\kappa_{11}} G_w^{(s)} + \sum_{j=1}^{M} \sum_{n=1}^{\infty} [B_n^j \eta_j^{-n} + C_n^j \bar{\eta}_j^{-n}] \quad (10)$$

Wherein, $H_n^{(1)}(*)$ is the first Hankel function. Introducing a mapping function: $\eta_j = \omega(\xi_j)$, then on the mathematical plane (ξ_j), the above expression can be written as [13]:

$$G_w^{(s)} = \sum_{j=1}^{M} \sum_{n=-\infty}^{\infty} A_n^j H_n^{(1)}(k|\omega(\xi_j)|) \cdot \left[\left(\frac{\omega(\xi_j)}{|\omega(\xi_j)|} \right)^n + \left(\frac{\omega(\xi_j)}{|\omega(\xi_j)|} \right)^{-n} \right]$$
$$G_\phi^{(s)} = \frac{e_{15}}{\kappa_{11}} G_w^{(s)} + \sum_{j=1}^{M} \sum_{n=1}^{\infty} \left[B_n^j \cdot \omega(\xi_j)^{-n} + C_n^j \cdot \overline{\omega(\xi_j)}^{-n} \right] \quad (11)$$

The coordinate transformation relation is:

$$\left.\begin{aligned} \eta &= \eta_j + c_j = \omega(\xi_j) + c_j \\ \eta_s &= \eta - c_s = \omega(\xi_j) + c_j - c_s \end{aligned}\right\} \quad (12)$$

Then, the expressions of G_w and G_f are:

$$G_w = G_w^{(i)} + G_w^{(s)}, \quad G_\phi = G_\phi^{(i)} + G_\phi^{(s)} \quad (13)$$

There is no displacement field but only electric field in the depression, and the expression of electric potential in the *j*-th depression should satisfy the Laplace equation $\nabla^2 G_\phi^{cj} = 0$. Considering that the electric potential in the cavity should be finite, its expression can be taken as follows:

$$G_\phi^{cj} = D_0 + \sum_{n=1}^{\infty} \left[D_n^j \cdot \eta_j^n + E_n^j \cdot \bar{\eta}_j^n \right] \quad (14)$$

On the mapping plane (ξ_j), the above formula can be transformed into the expression as:

$$G_\phi^{cj} = D_0 + \sum_{n=1}^{\infty} \left[D_n^j \cdot \omega(\xi_j)^n + E_n^j \cdot \overline{\omega(\xi_j)}^n \right] \quad (15)$$

Forest Chemicals Review
www.forestchemicalsreview.com
ISSN: 1520-0191
May-June 2022 Page No. 932-946
Article History: Received: 24 February 2022, Revised: 05 April 2022, Accepted: 08 May 2022, Publication: 30 June 2022

The coefficients A_n^j, B_n^j, C_n^j, D_n^j and E_n^j can be obtained from the boundary conditions of the *j*-th depression with arbitrary shape.

3.2 Scattering of SH wave by noncircular cavity

First, the infinite piezoelectric medium with only noncircular cavities and without cracks is considered. As shown in Fig 3, a steady SH wave is incident at an angle a_0 with the X axis.

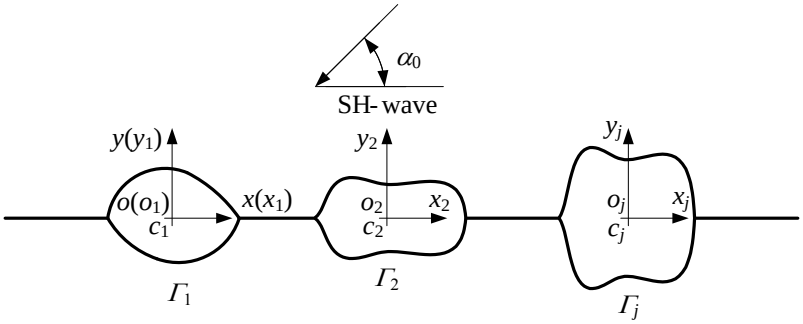

Fig 3: Scattering model of SH wave by multiple noncircular cavities in infinite piezoelectric material

The displacement field and electric potential field are composed of incident and scattering parts. Wherein, the expressions of $w^{(i)}$ and $f^{(i)}$ can be given by:

$$\begin{aligned} w^{(i)} &= w_0 \cdot \exp\left[-i\frac{k}{2}\left(\eta e^{-i\alpha_0} + \bar{\eta} e^{i\alpha_0}\right)\right] \\ \phi^{(i)} &= \frac{e_{15}}{\kappa_{11}} w^{(i)} \end{aligned} \tag{16}$$

Introducing the mapping function: $\eta_j = \omega(\xi_j)$, then on the mathematical plane (ξ_j), the above expression can be written as:

$$\begin{aligned} w^{(i)} &= w_0 \cdot \exp\left\{-i\frac{k}{2}\left[\left(\omega(\xi_j) + c_j\right)e^{-i\alpha_0} + \overline{\left(\omega(\xi_j) + c_j\right)}e^{i\alpha_0}\right]\right\} \\ \phi^{(i)} &= \frac{e_{15}}{\kappa_{11}} w^{(i)} \end{aligned} \tag{17}$$

The scattered displacement field $w^{(s)}$ and the electric potential field $f^{(s)}$ generated by the cavities can be given by:

Forest Chemicals Review
www.forestchemicalsreview.com
ISSN: 1520-0191
May-June 2022 Page No. 932-946
Article History: Received: 24 February 2022, Revised: 05 April 2022, Accepted: 08 May 2022, Publication: 30 June 2022

$$w^{(s)} = \sum_{j=1}^{M}\sum_{n=-\infty}^{\infty} {}^{j}A_n^s H_n^{(1)}(k|\omega(\xi_j)|)\left(\frac{\omega(\xi_j)}{|\omega(\xi_j)|}\right)^n$$
$$\phi^{(s)} = \frac{e_{15}}{\kappa_{11}} w^{(s)} + \sum_{j=1}^{M}\sum_{n=1}^{+\infty} {}^{j}B_n^s \omega(\xi_j)^{-n} + \sum_{j=1}^{M}\sum_{n=1}^{+\infty} {}^{j}C_n^s \overline{\omega(\xi_j)}^{-n} \quad (18)$$

The expressions of the total displacement $w^{(t)}$ and the electric potential $f^{(t)}$ which in the infinite piezoelectric material with multiple noncircular cavities can be given by:

$$w^{(t)} = w^{(i)} + w^{(s)}, \quad \phi^{(t)} = \phi^{(i)} + \phi^{(s)} \quad (19)$$

The electric potential ϕ_j^c meeting the control equation $\nabla^2\phi_j^c = 0$ in the *j*-th noncircular cavity is:

$$\phi_j^c = {}^{j}D_0^s + \sum_{n=1}^{\infty}\left[{}^{j}D_n^s \omega(\xi_j)^n + {}^{j}E_n^s \overline{\omega(\xi_j)}^n \right] \quad (20)$$

The infinite algebraic equations to solve the coefficients ${}^{j}A_n^s$, ${}^{j}B_n^s$, ${}^{j}C_n^s$, ${}^{j}D_n^s$ and ${}^{j}E_n^s$ in equations (18) and (20) are obtained from the boundary conditions at the *j*-th noncircular cavity. Based on the orthogonality of periodic functions and the convergence of cylindrical functions, the equations can be solved by the linear algebra theory.

3.3 Problem solving

Using the crack-division technique combined with the conjunction method, we can construct a model of SH wave scattering by radial collinear conducting cracks at multiple noncircular cavity edges in piezoelectric medium. The conjunction process is displayed in the following diagrammatic map.

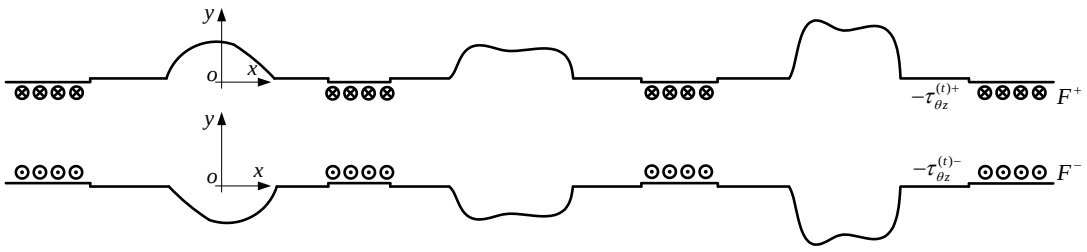

Fig 4: Cutting and section fitting of cracks in piezoelectric medium

Firstly, the infinite piezoelectric medium with multiple noncircular cavities is cut along the X axis. The upper section contains displacement $w^{(t+)}$ and stress $\tau_{\theta z}^{(t)+}$, while the lower section contains displacement $w^{(t-)}$ and stress $\tau_{\theta z}^{(t)-}$. Next, the stresses $[-\tau_{\theta z}^{(t)+}]$ and $[-\tau_{\theta z}^{(t)-}]$ are applied to the upper and lower sections of the corresponding areas where cracks are to occur, so that the combined stresses of these corresponding

Forest Chemicals Review
www.forestchemicalsreview.com
ISSN: 1520-0191
May-June 2022 Page No. 932-946
Article History: Received: 24 February 2022, Revised: 05 April 2022, Accepted: 08 May 2022, Publication: 30 June 2022

areas are zero. That is, conductive cracks are formed. To ensure the continuity conditions in the area outside the noncircular cavities and cracks on the sectioning surface, a pair of external forces F^+ and F^- should be applied in this area. Finally, the upper and lower halves of infinite piezoelectric media are joined together, and the stress continuity condition on the sectioning surface is as follows:

$$\tau_{\theta z}^{(t)+} + F^+ = \tau_{\theta z}^{(t)-} + F^- \tag{21}$$

The condition for displacement continuity is:

$$w^{(t+)} + w^{(F+)} + w^{(c+)} = w^{(t-)} + w^{(F-)} + w^{(c-)} \tag{22}$$

Wherein, $w^{(t+)} = w^{(t-)} = w^{(t)}$,

$$w^{(F+)} = \int_{\Gamma_0} F^+(r_0,\theta_{0L}) G_w(r,\theta;r_0,\theta_{0L}) dr_0 + \sum_{j=1}^{M-1} \int_{\Gamma_j} F^+(r_0,\theta_{0R}) G_w(r,\theta;r_0,\theta_{0R}) dr_0 + \int_{\Gamma_N} F^+(r_0,\theta_{0R}) G_w(r,\theta;r_0,\theta_{0R}) dr_0$$

$$w^{(F-)} = -\int_{\Gamma_0} F^-(r_0,\theta_{0L}) G_w(r,\theta;r_0,\theta_{0L}) dr_0 - \sum_{j=1}^{M-1} \int_{\Gamma_j} F^-(r_0,\theta_{0R}) G_w(r,\theta;r_0,\theta_{0R}) dr_0 - \int_{\Gamma_N} F^-(r_0,\theta_{0R}) G_w(r,\theta;r_0,\theta_{0R}) dr_0$$

$$w^{(c+)} = \int_{\Pi_1} \tau_{\theta z}^{(t)}(r_0,\theta_{0L}) G_w(r,\theta;r_0,\theta_{0L}) dr_0 - \int_{\Pi_2} \tau_{\theta z}^{(t)}(r_0,\theta_{0R}) G_w(r,\theta;r_0,\theta_{0R}) dr_0 - \sum_{j=2}^{M} \int_{\Pi_{2j-1}} \tau_{\theta z}^{(t)}(r_0,\theta_{0R}) G_w(r,\theta;r_0,\theta_{0R}) dr_0 - \sum_{j=2}^{M} \int_{\Pi_{2j}} \tau_{\theta z}^{(t)}(r_0,\theta_{0R}) G_w(r,\theta;r_0,\theta_{0R}) dr_0$$

$$w^{(c-)} = -\int_{\Pi_1} \tau_{\theta z}^{(t)}(r_0,\theta_{0L}) G_w(r,\theta;r_0,\theta_{0L}) dr_0 + \int_{\Pi_2} \tau_{\theta z}^{(t)}(r_0,\theta_{0R}) G_w(r,\theta;r_0,\theta_{0R}) dr_0 + \sum_{j=2}^{M} \int_{\Pi_{2j-1}} \tau_{\theta z}^{(t)}(r_0,\theta_{0R}) G_w(r,\theta;r_0,\theta_{0R}) dr_0 + \sum_{j=2}^{M} \int_{\Pi_{2j}} \tau_{\theta z}^{(t)}(r_0,\theta_{0R}) G_w(r,\theta;r_0,\theta_{0R}) dr_0$$

Here, $\theta_{0L} = \pi$; $\theta_{0R} = 0$; $\Gamma_0 \in [a_1 + A_1, \infty]$; $\Gamma_j \in [C_j + a_{2j} + A_{2j}, C_j + a_{2j} + A_{2j} + d_j]$; $\Gamma_N \in [C_N + a_{2N} + A_{2N}, \infty]$; $\Pi_1 \in [a_1, a_1 + A_1]$; $\Pi_2 \in [a_2, a_2 + A_2]$; $\Pi_{2j-1} \in [C_j - a_{2j-1} - A_{2j-1}, C_j - a_{2j-1}]$; $\Pi_{2j} \in [C_j + a_{2j}, C_j + a_{2j} + A_{2j}]$; wherein, C_j is the distance from the origin of the whole coordinate system to the center of each noncircular

Forest Chemicals Review
www.forestchemicalsreview.com
ISSN: 1520-0191
May-June 2022 Page No. 932-946
Article History: Received: 24 February 2022, Revised: 05 April 2022, Accepted: 08 May 2022, Publication: 30 June 2022

cavity, $a_{2j\text{-}1}$ and a_{2j} represent the distance from the left end point and right end point of the noncircular cavity along the X axis to the defect center respectively, and $j = 1, 2, \cdots, \mathrm{M}$.

Based on the equations (21) and (22) and in combination with the above equations, the definite solution integral equations for solving the unknown force system $F(r_0, \theta_0)$ can be obtained:

$$\begin{aligned}
&\int_{\Gamma_0} F^+(r_0, \theta_{0L}) G_w(r, \theta; r_0, \theta_{0L}) dr_0 + \sum_{j=1}^{\mathrm{M}-1} \int_{\Gamma_j} F^+(r_0, \theta_{0R}) G_w(r, \theta; r_0, \theta_{0R}) dr_0 \\
&+ \int_{\Gamma_N} F^+(r_0, \theta_{0R}) G_w(r, \theta; r_0, \theta_{0R}) dr_0 = -\int_{\Pi_1} \tau_{\theta z}^{(t)}(r_0, \theta_{0L}) G_w(r, \theta; r_0, \theta_{0L}) dr_0 \\
&+ \int_{\Pi_2} \tau_{\theta z}^{(t)}(r_0, \theta_{0R}) G_w(r, \theta; r_0, \theta_{0R}) dr_0 + \sum_{j=2}^{\mathrm{M}} \int_{\Pi_{2j-1}} \tau_{\theta z}^{(t)}(r_0, \theta_{0R}) G_w(r, \theta; r_0, \theta_{0R}) dr_0 \\
&+ \sum_{j=2}^{\mathrm{M}} \int_{\Pi_{2j}} \tau_{\theta z}^{(t)}(r_0, \theta_{0R}) G_w(r, \theta; r_0, \theta_{0R}) dr_0 \qquad \theta = 0, \pi
\end{aligned} \tag{23}$$

The direct numerical integration method is adopted in combination with the attenuation characteristics of scattered waves. The above integral equations can be transformed into the finite linear algebraic equation groups to solve the value of additional external force system at discrete points.

The dynamic stress intensity factor is introduced, and its expression is:

$$k_{\mathrm{III}} = \lim_{r_0 \to S_j} F(r_0, \theta_0) \cdot \sqrt{2(r_0 - S_j)} \tag{24}$$

Wherein, $S_j = C_j + a_{2j} + A_{2j}$ or $C_j - a_{2j-1} - A_{2j-1}$.

For the convenience of solving, substituting the integrand function in equation (24) at the crack tip as follows:

$$\begin{aligned}
F \cdot G_w &= \lim_{r_0 \to S_j} \left[F \cdot \sqrt{2(r_0 - S_j)} \right] \cdot \left[G_w \Big/ \sqrt{2(r_0 - S_j)} \right] \\
&= k_{\mathrm{III}} \cdot \left[G_w \Big/ \sqrt{2(r_0 - S_j)} \right]
\end{aligned} \tag{25}$$

Defining a dimensionless factor k_3^{σ}, namely

$$k_3^{\sigma} = \left| \frac{k_{\mathrm{III}}}{\tau_0 Q} \right| \tag{26}$$

Forest Chemicals Review
www.forestchemicalsreview.com
ISSN: 1520-0191
May-June 2022 Page No. 932-946
Article History: Received: 24 February 2022, Revised: 05 April 2022, Accepted: 08 May 2022, Publication: 30 June 2022

Wherein, τ_0 is the stress amplitude $\tau_0 = c^* k w_0$ of incident wave. Q is a characteristic parameter, and it takes the following expression in piezoelectric material which contains radial collinear cracks generating from the edge of noncircular cavities:

$$Q = \sqrt{\frac{A_{2j-1} + a_{2j-1} + a_{2j} + A_{2j}}{2}} \tag{27}$$

Ⅳ. RESULTS AND DISCUSSION

As an example, in the case of double elliptical cavities, this paper gives the numerical results of the change of k_3^σ at the inner end point of the radial collinear double cracks (shown by point P in Fig 5) emanating from elliptical cavities with the size of the major and minor axes, the length of cracks, incident wave frequency and piezoelectric constant. Among it, it is assumed that the size of two elliptical cavities and the length of cracks are equal. They are indicated by a, b and A respectively.

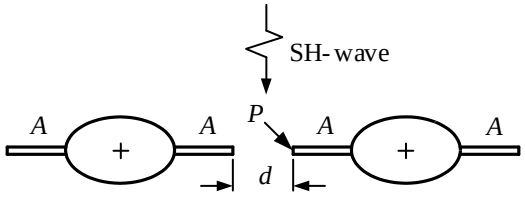

Fig 5: Calculation model of radial double cracks emanating from elliptical cavities

Fig 6 shows the change of k_3^σ with dimensionless wave number ka when b/a takes different values. It is found that when b/a=0.001, that is, when it degenerates into two linear crack models, its value basically agrees with the data in references [4][14], and the error remains within 1.5%. In other cases, the k_3^σ value curve oscillates and attenuates with the increase of ka, and the maximum value is obtained around ka=0.3. When ka<0.3, the value of k_3^σ gradually increases with the increase of b/a, while when ka>0.8, its changing trend is just opposite.

Fig 7 shows the change of k_3^σ with dimensionless wave number ka when A/a takes different values. It is found that the k_3^σ value curve reaches its peak at low frequency ka=0.25 or so, and its value oscillation decreases with the increase of incident frequency. When ka<0.3 or so, k_3^σ value curves increase with the increase of A/a, and when ka>0.3, k_3^σ value curves have different sizes. Therefore, in the low frequency band, when the crack size is not much different from the semi-major axis, the elliptical cavity has obvious influence on k_3^σ value.

Forest Chemicals Review
www.forestchemicalsreview.com
ISSN: 1520-0191
May-June 2022 Page No. 932-946
Article History: Received: 24 February 2022, Revised: 05 April 2022, Accepted: 08 May 2022, Publication: 30 June 2022

Fig 8 shows the change of k_3^σ value with dimensionless wave number *ka* when *d*/*a* is different. It can be seen that when *ka*<1.5, the value of k_3^σ increases with the decrease of *d*/*a*, and the maximum value obtained around *ka*=0.25. After entering the high frequency band, k_3^σ value oscillation decreases.

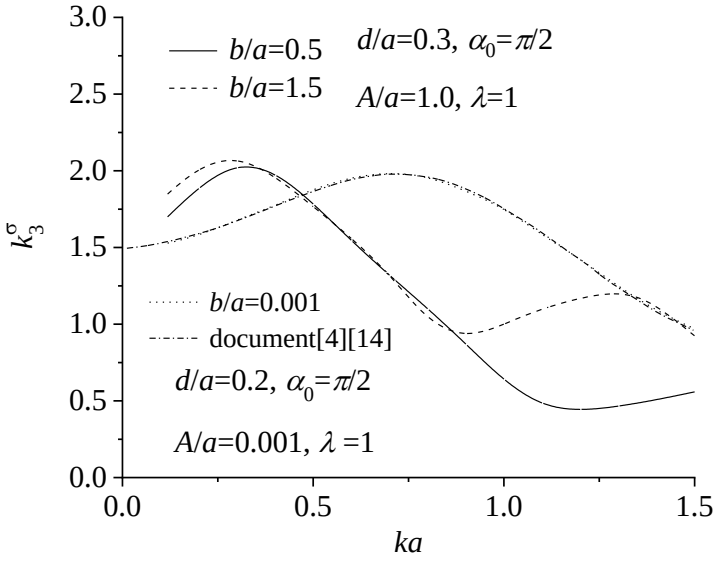

Fig 6: The change of k_3^σ value with *ka* when *b*/*a* takes different values

Fig 9 shows the change of k_3^σ value with *b*/*a* at low frequency *ka*=0.5 when *A*/*a* takes different values. It can be seen that the k_3^σ value of the curve of *A*/*a* =1.0 is larger than that of the other two cases, which shows that when the length of crack and the semi-major axis have the nearly same value, the phenomena of dynamic stress concentration are more obvious.

Fig 10 shows the change of k_3^σ value with *b*/*a* at *ka*=1.0 when *d*/*a* takes different values. It can be found that with the higher value of *b*/*a*, the k_3^σ value of each curve gradually increases at the range *b*/*a*<1.65, and the k_3^σ reaches the peak value around *b*/*a*=1.65.

Figure 11 shows the change of k_3^σ value with dimensionless wave number *ka* when *l* takes different values. It can be seen from the figure that k_3^σ curves all reach maximum values around the wave number *ka*=0.3, and their values increase with the increase of *b*/*a*. When 0.6<*ka*<1.1, the value of k_3^σ decreases with the higher value of *b*/*a*. The curves of k_3^σ have a similar changing trend with the increase of *ka*.

Forest Chemicals Review
www.forestchemicalsreview.com
ISSN: 1520-0191
May-June 2022 Page No. 932-946
Article History: Received: 24 February 2022, Revised: 05 April 2022, Accepted: 08 May 2022, Publication: 30 June 2022

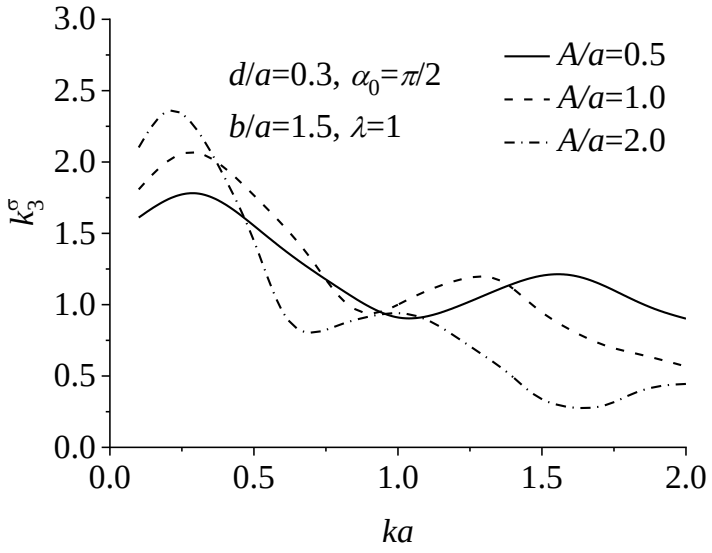

Fig 7: The change of k_3^σ value with *ka* when *A*/*a* takes different values

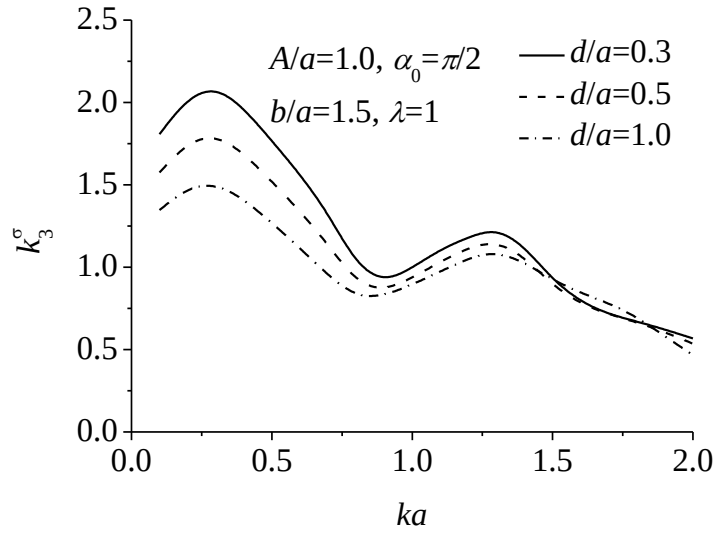

Fig 8: The change of k_3^σ value with *ka* when *d*/*a* takes different values

Forest Chemicals Review
www.forestchemicalsreview.com
ISSN: 1520-0191
May-June 2022 Page No. 932-946
Article History: Received: 24 February 2022, Revised: 05 April 2022, Accepted: 08 May 2022, Publication: 30 June 2022

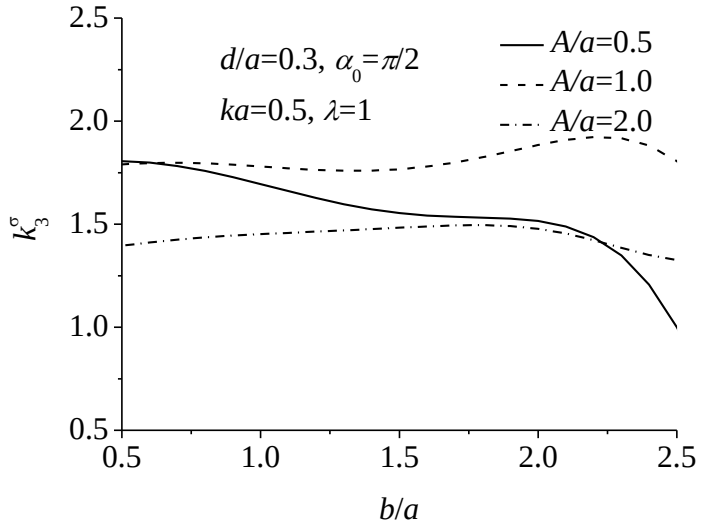

Fig 9: The change of k_3^σ value with b/a when A/a takes different values

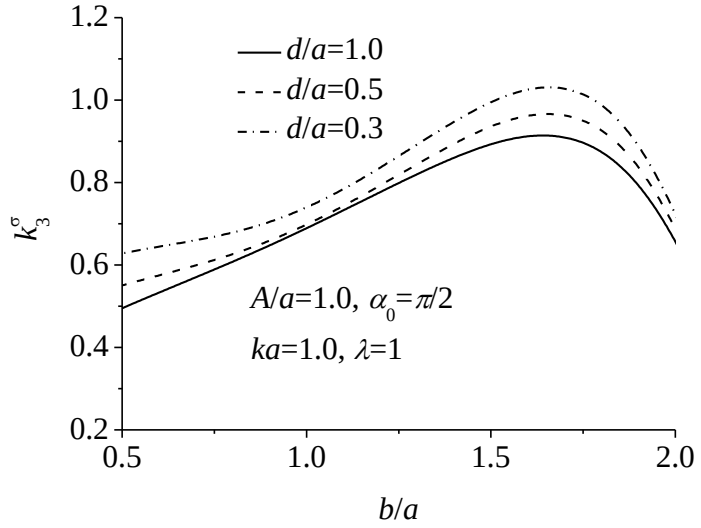

Fig 10: The change of k_3^σ value with b/a when d/a takes different values

Forest Chemicals Review
www.forestchemicalsreview.com
ISSN: 1520-0191
May-June 2022 Page No. 932-946
Article History: Received: 24 February 2022, Revised: 05 April 2022, Accepted: 08 May 2022, Publication: 30 June 2022

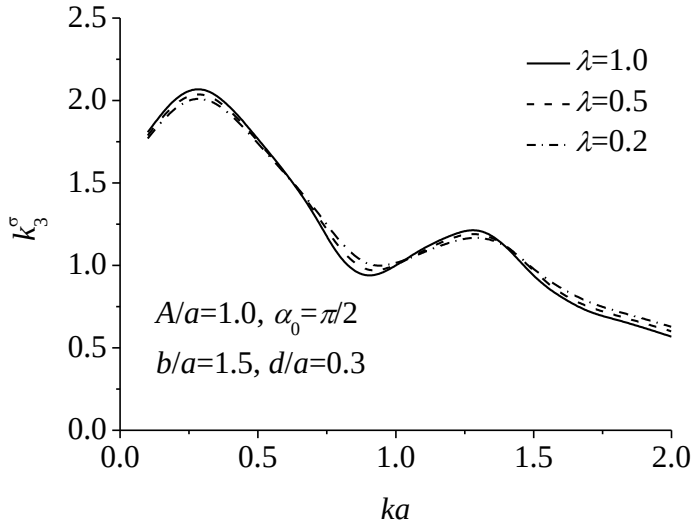

Fig 11: The change of k_3^σ value with *ka* when *l* takes different values

Ⅴ. CONCLUSIONS

In this paper, the dynamic stress concentrations of the tip of radial collinear cracks generating from multiple noncircular cavities in piezoelectric medium which subjected to SH waves are studied by using complex variable function method, conformal mapping technology, crack-division technique and conjunction method. It is found that the maximum dynamic stresses are obtained about *ka*=0.3, and the damping of oscillations of the stress concentrations at the cracks' tip are appeared with the variation of *ka*. So the dynamic antiplane analysis is more important in the lower frequency. When the lengths of cracks are about the same as the semi-major axis, the dynamic stress concentration is more obvious, and its value tends to decrease with the higher value of *l*. The smaller the range between multiple cracks is, the more obvious the interaction between defects is, and the larger the k_3^σ value is. Therefore, considering the geometric parameters and physical parameters of piezoelectric structures comprehensively, the possibility of structural damage can be reduced by selecting the appropriate combination.

This paper provides a useful theoretical approach to analyze and solve this kind of problems. It can be found that according to analyze the recent research works, there are also some shortcomings in this field of investigation, such as the particularity of defects. At present, the dynamic fracture mechanics of piezoelectric material is not very mature, and the existing theoretical models can not fully explain the phenomena observed in the experiment and practical engineering, so we need to make beneficial explorations in the theory study field.

Forest Chemicals Review
www.forestchemicalsreview.com
ISSN: 1520-0191
May-June 2022 Page No. 932-946
Article History: Received: 24 February 2022, Revised: 05 April 2022, Accepted: 08 May 2022, Publication: 30 June 2022

REFERENCES

[1] Du JK, Shen YP, Wang X (2002) Scattering of anti-plane shear waves by a partially debonded piezoelectric circular cylindrical inclusion. Acta Mechanica 158: 169-182
[2] Feng W, Wang L, Jiang Z, Zhao Y (2004) Shear wave scattering from a partially debonded piezoelectric cylindrical inclusion. Acta Mechanica Solida Sinica 17(3): 258-269
[3] Hu K, Meguid SA, Wang L et al. (2021) Electro-elastic field of a piezoelectric quasicrystal medium containing two cylindrical inclusions. Acta Mechanica 232: 2513-2533
[4] Wang XD (2001) On the dynamic behavior of interacting interfacial cracks in piezoelectric media. International Journal of Solids and Structures 38: 815-831
[5] Wu TH, Li XY (2019) Elliptical crack problem in magneto-electro-thermo-elasticity of transversely isotropic materials: 3D analytical and numerical solutions. International Journal of Engineering Science 144: 103136
[6] Zheng RF, Wu TH, Li XY (2019) Elliptic crack in transversely isotropic magneto-electro-elasticity under shear loading. International Journal of Engineering Science 134: 47-65
[7] Hu KQ, Zhong Z, Chen ZT (2019) Interface crack between magnetoelectroelastic and orthotropic half-spaces under anti-plane loading. Theoretical and Applied Fracture Mechanics 99: 95-103
[8] García-Sánchez F, Rojas-Díaz R, Sáez A, Zhang C (2007) Fracture of magneto-electroelastic composite materials using boundary element method (BEM). Theoretical and Applied Fracture Mechanics 47: 192-204
[9] Guo JH, Lu ZX, Han HT, Yang ZY (2009) The behavior of two non-asymmetrical permeable cracks emanating from an elliptical hole in a piezoelectric solid. European Journal of Mechanics A/Solids 46: 3799-3809
[10] Xiao JH, Xu YL, Zhang FC (2018) Fracture characteristics of a cracked equilateral triangle hole with surface effect in piezoelectric materials. Theoretical and Applied Fracture Mechanics 96: 476-482
[11] Feng GY, Xiao JH, Su MY (2020) Fracture mechanics analysis of mode-Ⅲ radial multi cracks on the edge of a hole with surface effects. Applied Mathematics and Mechanics 41(4): 376-385
[12] Bleustein JL (1968) A new surface wave in piezoelectric materials. Applied Physics letter 13: 412-413
[13] Gai BZ (1986) Diffraction of elastic waves in the plane multiply-connected region and dynamic stress concentration. Applied Mathematics and Mechanics 7(1): 25-36
[14] Wang XD, Meguid SA (2000) Modelling and analysis of the dynamic behaviour of piezoelectric materials containing interacting cracks. Mechanics of Materials 32: 723-737